Coordination Polymers

DOI: 10.1002/anie.200803387

Modular Synthesis of Functional Nanoscale Coordination Polymers

Wenbin Lin, William J. Rieter, and Kathryn M. L. Taylor*

biomedical imaging · coordination polymers · drug delivery · metal-organic frameworks · nanoparticles

The coordination-directed assembly of metal ions and organic bridging ligands has afforded a variety of bulk-scale hybrid materials with promising characteristics for a number of practical applications, such as gas storage and heterogeneous catalysis. Recently, so-called coordination polymers have emerged as a new class of hybrid nanomaterials. Herein, we highlight advances in the syntheses of both amorphous and crystalline nanoscale coordination polymers. We also illustrate how scaling down these materials to the nano-regime has enabled their use in a broad range of applications including catalysis, spin-crossover, templating, biosensing, biomedical imaging, and anticancer drug delivery. These results underscore the exciting opportunities of developing next-generation functional nanomaterials based on molecular components.

1. Introduction

Technological advancements have led to new and exciting applications for materials that might have once been thought inconceivable. This statement holds particularly true for the rapidly developing field of nanotechnology. The unique size-dependent properties of materials on the nanometer-scale have led to their applications in many areas, including catalysis,[1] wavelength-tunable lasers,[2] solar cells,[3] bioimaging,[4] and drug delivery.[5] Whereas the vast majority of nanomaterials are either purely inorganic or organic in composition, the combination of metal and organic components at the molecular level has recently afforded a new class of highly tailorable hybrid nanomaterials known as nanoscale coordination polymers.

Coordination polymers or metal-organic frameworks are built from metal ions or metal ion clusters that have two or more vacant coordination sites and polydentate bridging ligands. Prussian blue and mixed-metal cyanometallates are the classic examples of coordination polymers.[6] Numerous reports on the syntheses and characterization of cyanometallate nanoparticles (Figure 1) have been published over the last decade,[7] and they exhibit unique size-dependent properties such as superparamagnetism,[7a] photo-induced superparamagnetism,[7b] and spin-glass-like behavior.[7c] Coordination polymers however are not limited to the cyanometallates, and can be synthesized from a wide range of metal and organic building blocks. The tunable nature of coordina-

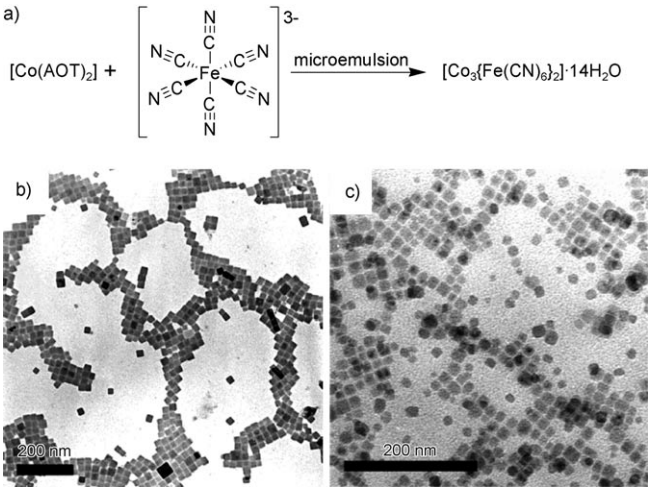

Figure 1. a) Scheme illustrating the synthesis of cyanometallate nanoparticles. b) and c) TEM (transmission electron microscopy) images of cyanometallate nanoparticles synthesized in $Co(AOT)_2$ water-in-oil microemulsions at $W = 30$ and $W = 10$, respectively.[7b] Scale bar = 200 nm. AOT = sodium bis(2-ethylhexyl) sulphosuccinate; W = water/surfactant molar ratio.

[*] Prof. Dr. W. Lin, Dr. W. J. Rieter, K. M. L. Taylor
Department of Chemistry, CB#3290, University of North Carolina, Chapel Hill, NC 27599 (USA)
Fax: (+1) 919-962-2388
E-mail: wlin@unc.edu

tion polymers has allowed them to be engineered for a number of bulk-scale applications, including gas storage,[8a] catalysis,[8b] and nonlinear optics.[8c] By scaling them down to the nanometer-regime, the scope of cyanometallate nanoparticles will be vastly expanded, which, in turn, will lead to a new generation of functional nanostructures. Herein, we present recent advances in the syntheses of nanoscale coordination polymers, and illustrate the application of this exciting new class of nanomaterials in many areas, ranging from heterogeneous catalysis to anticancer drug delivery.

2. Synthesis of Nanoscale Coordination Polymers

2.1. Classification of Nanoscale Coordination Polymers

Nanoscale coordination polymer particles can be divided into two main classes, based on their structural regularity/crystallinity: the amorphous class, that is denoted as NCPs, and the crystalline class, known as nanoscale metal-organic frameworks (NMOFs). NCPs typically adopt a spherical morphology to minimize the interfacial free energy between the particles and solvent. Conversely, the morphologies of NMOFs are controlled by both the intrinsic crystal structures and their interactions with solvent molecules. NMOFs tend to adopt well-defined, non-spherical morphologies, suggesting the predominance of crystal lattice energy over particle/solvent interactions. The crystalline nature of NMOFs allows for an exact understanding of their compositions and structures, and greatly facilitates the delineation of composition, structure, and property interrelationships in this class of nanostructures.

2.2. Synthesis of Amorphous Nanoscale Coordination Polymers

NCPs are generally synthesized by exploiting the insolubility of the particles in a given solvent system. Wang et al. reported the first synthesis of non-cyanometallate NCPs in 2005.[9] The authors discovered that submicrometer-scale spherical colloids could be prepared by simply mixing H_2PtCl_6 and *p*-phenylenediamine in aqueous solution. From a 0.50 mM solution of the reagents, they isolated monodisperse spheres of approximately 420 nm in diameter, taking advantage of the very low solubility in water of the product from the reaction between the two components.

Sweigart, Son and co-workers also used this approach to formulate particles consisting of $[(\eta^6\text{-}1,4\text{-hydroquinone})Rh(cod)]^+$ linkers and Al^{3+} metal-ion connectors.[10] Addition of $Al(OiPr)_3$ to a solution of the organorhodium complex in THF immediately led to the precipitation of nanoparticles with an average diameter of 340 nm (Scheme 1). They further

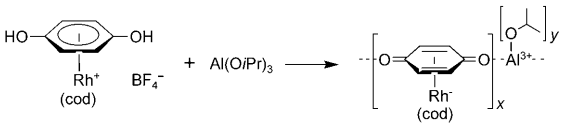

Scheme 1. Synthesis of an organometallic nanocatalyst.[10]

showed that the particle sizes increased as the reagent concentrations increased, suggesting that the particle growth rates have an influence of the on their sizes. This synthetic strategy is reminiscent of those used for the synthesis of highly enantioselective zirconium phosphonate-based heterogeneous asymmetric catalysts with ill-defined morphologies.[11]

Mirkin and co-workers described a different approach toward NCPs by precipitating particles from a precursor solution of the components, by addition of a poor solvent.[12] NCPs based on metal and homochiral carboxylate-functionalized bis-metallo-tridentate Schiff base (BMSB) building blocks were, for example, prepared by adding a poor, initiating solvent, such as diethyl ether or pentane, to a solution of the metal and BMSB components in pyridine (Scheme 2). Whereas slow diffusion of the poor solvent into the precursor solution resulted in micron-sized particles, its rapid addition gave much smaller NCPs. These results were significant because they showed that growth processes could be quenched at an early stage of the reaction.

Wenbin Lin obtained his BS and PhD degrees from University of Science and technology of China (Hefei) in 1988 and the University of Illinois at Urbana-Champaign in 1994, respectively. After a NSF postdoctoral fellowship at Northwestern University, he became assistant professor of Chemistry at Brandeis University in 1997. He moved to the University of North Carolina at Chapel Hill in 2001, and was promoted to associate and full professor of chemistry in 2003 and 2007, respectively. His research focuses on designing hybrid nanomaterials for applications in chemical and life sciences.

William J. Rieter was born in Salisbury, MD, USA in 1982. He received a BS in biochemistry and a BA in chemistry from the College of Charleston in 2004. He was a NSF Predoctoral Fellow at the University of North Carolina at Chapel Hill, where he received his PhD with Prof. W. Lin in 2008. He is currently pursuing a doctorate in medicine at the Medical University of South Carolina.

Kathryn M. L. Taylor was born in Upper Heyford, Oxfordshire, England in 1982. She received a BS in chemistry from the College of William and Mary in 2004. She is currently pursuing a doctorate in chemistry at the University of North Carolina at Chapel Hill with Prof. Wenbin Lin. Her current research is focused on the development of hybrid nanoparticles for biomedical applications.

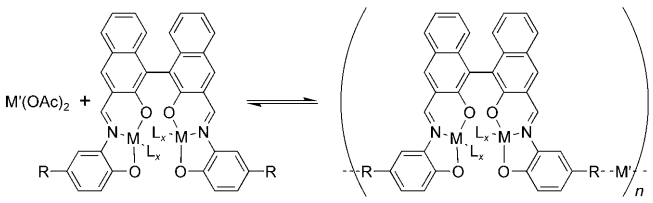

Scheme 2. Synthesis of NCPs based on the M–BMSB building block.[12]

Lin et al. recently used a similar strategy to formulate NCPs composed of the anticancer drug disuccinatocisplatin (DSCP) and Tb^{III}.[13] In the synthesis, the pH value of an aqueous solution of $TbCl_3$ and di(methylammonium) DSCP was adjusted to approximately 5.5 with dilute aqueous NaOH (Scheme 3). Methanol was then quickly poured into the

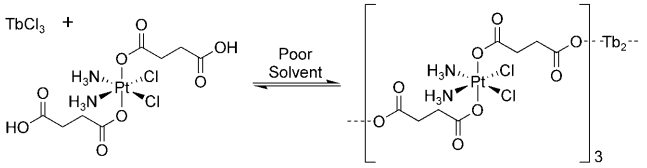

Scheme 3. Synthesis of NCPs based on the anticancer drug disuccinatocisplatin (DSCP).[13]

precursor solution to induce the formation of NCPs with a diameter of (58 ± 11.3) nm. Careful control of the pH of the aqueous precursor solution was critical for the successful and reproducible synthesis of NCPs in this system.

NCPs have also been prepared from the assembly of 1D coordination oligomers. These NCPs are distinct because of the initial formation of defined linear chain complexes (high oligomers) in solution. For instance, Maeda and co-workers noted that treatment of dipyrrin "dimers" with $Zn(OAc)_2$ in THF resulted in a color change indicative of coordination between Zn ions and dipyrrin units (Scheme 4).[14] Uniform nanoparticles were generated using a carefully chosen initial concentration of the components, presumably by the assembly of pre-formed oligomeric species into NCPs. They also studied the structural effects of the dimers on nanoparticle

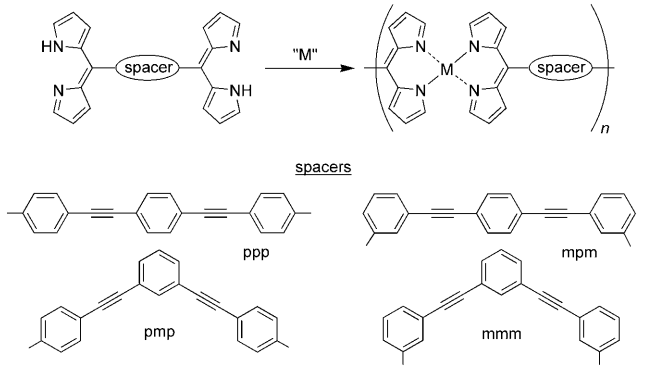

Scheme 4. Examples of various dipyrrin "dimers" used to synthesize NCPs by Maeda et al.[14]

formation, and proposed a multi-step sequence for NCP particle formation that is akin to the protein folding process.

Similarly, Ruiz-Molina and co-workers prepared NCPs based on 1D oligomers by rapidly adding water to a solution of $Co(OAc)_2$, 3,5-di-*tert*-butyl-1,2-catechol (dbcat), and 1,4-bis(imidazol-1-ylmethyl)benzene (bix) in an ethanol/water mixture (Figure 2).[15] The size of the particles was tuned from

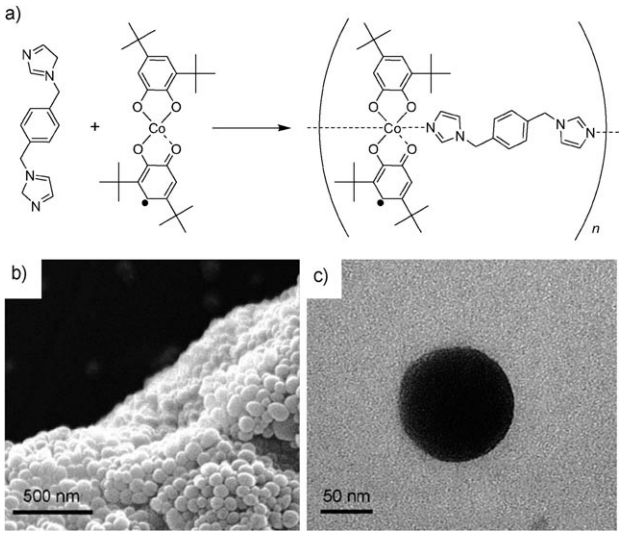

Figure 2. a) Scheme for the synthesis of valence-tautomeric nanoparticles. b) SEM (scanning electron microscopy) and c) TEM micrographs of valence-tautormeric nanoparticles.[15]

(76 ± 9) nm to (204 ± 13) nm, by varying the rate at which the water was added from 50 to 0.07 $mL\,s^{-1}$, to precipitate the particles . These results again illustrate the ability to control the particle-growth processes by quenching with a poor solvent.

2.3. Synthesis of Nanoscale Metal-Organic Frameworks

The amorphous nature of NCPs prohibits a detailed understanding of these systems at a molecular level, and can lead to additional variability in the compositions, size distributions, and morphologies between different experiments. Several distinct approaches have recently been developed for the synthesis of crystalline NMOFs, including water-in-oil microemulsions, surfactant-mediated hydrothermal syntheses, and high-temperature routes. Single crystal X-ray diffraction studies of the bulk MOFs provide an unequivocal understanding of the composition and structure of the nanoparticles, greatly facilitating characterization of NMOFs.

The ability to control the sizes of cyanometallate nanoparticles using water-in-oil microemulsions provided the inspiration to utilize this methodology for NMOF synthesis. Water-in-oil, or reverse, microemulsions are highly tailorable systems that consist of nanometer-sized water droplets stabilized by a surfactant in a predominantly organic phase. The micelles in the microemulsion essentially act as "nanoreactors" that assist in controlling the kinetics of particle

nucleation and growth. The size and number of micelles within the microemulsion can be tuned by varying the water to surfactant ratio (W).

Lin et al. prepared $Ln_2(bdc)_3(H_2O)_4$ NMOFs ($Ln = Eu^{3+}$, Gd^{3+}, or Tb^{3+} and bdc = 1,4-benzenedicarboxylate) by reacting $LnCl_3$ and di(methylammonium) BDC in the cationic cetyltrimethylammonium bromide (CTAB)/isooctane/1-hexanol/water microemulsion system (Figure 3a–b).[16] Nanorods

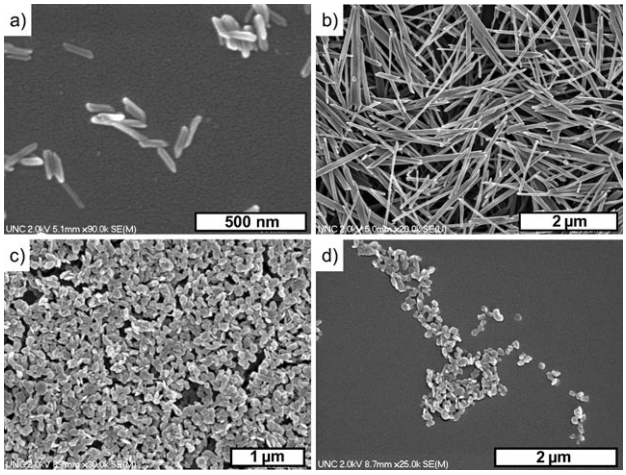

Figure 3. a) and b) SEM micrographs of $Gd_2(bdc)_3(H_2O)_4$ nanoparticles synthesized using a reverse microemulsion with $W = 5$ and $W = 10$, respectively. c) and d) SEM micrographs of $[Gd(itbc)(H_2O)_3]\cdot H_2O$.[16]

of fairly uniform size were isolated in high yield. By varying W from 5 to 10, the sizes of the nanorods could be tuned from approximately 125 nm in length by 40 nm in width to approximately 2 μm in length by 100 nm in width. The rod-like shape of the nanoparticles reflects the anisotropies associated with the growth of the nanocrystals. Higher W values lead to particles with higher aspect ratios resulting from a decrease of nucleation sites within the microemulsion. Moreover, the particle size decreased as the reactant concentrations were increased, presumably because more micelles were occupied by the reactants to generate more nucleation sites, leading to a reduction of particle sizes.

$[Ln(itbc)(H_2O)_3]\cdot H_2O$ NMOFs ($itbc$ = 1,2,4-benzenetricarboxylate) were similarly prepared by stirring a mixture of $LnCl_3$ and tri(methylammonium) $itbc$ in a CTAB/isooctane/1-hexanol/water microemulsion mixture (Figure 3c,d). Nanoplates with an average diameter of approximately 100 nm were isolated from a microemulsion of $W = 15$, when excess metal was used in the reaction.

NMOFs based on Mn^{2+} connectors and bdc and 1,3,5-benzenetricarboxylate (btc) bridging ligands were also synthesized in reverse microemulsions (Figure 4).[17] NMOFs of $Mn(bdc)(H_2O)_2$ were isolated as long rods, with a structure corresponding to a known crystalline phase. NMOFs of $Mn_2(btc)_3(H_2O)_6$ were isolated as crystalline spiraling rods, but their structure did not correspond to any known phase of Mn–btc-based MOFs.

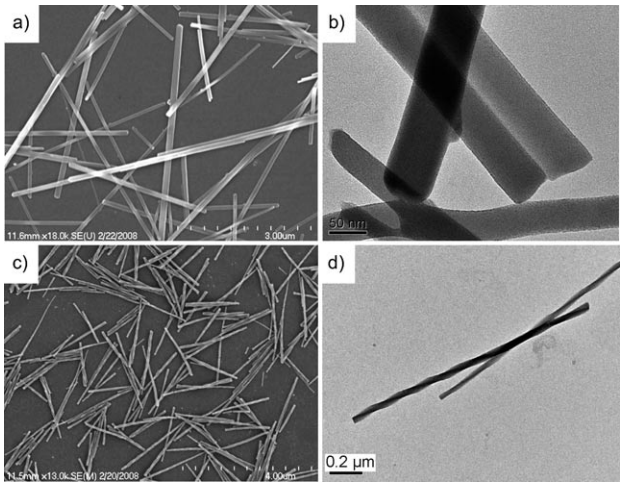

Figure 4. a) SEM and b) TEM micrographs of crystalline $Mn(bdc)(H_2O)_2$. c) SEM and d) TEM micrographs of crystalline $Mn_3(btc)_2(H_2O)_6$.[17]

Using a similar microemulsion-based method, Coronado et al. recently prepared spherical nanoparticles based on a 1D polymeric structure with the formula $[Fe(Htrz)_2(trz)](BF_4)$ (where Htrz is 1,2,4-1*H*-triazole).[18] Nanoparticles with a diameter of (11 ± 5) nm were obtained by mixing $Fe(BF_4)_3\cdot H_2O$, behenic acid, and Htrz in a microemulsion composed of the anionic surfactant sodium dioctyl sulfosuccinate (NaAOT), octane, and water.

Whereas room-temperature microemulsion synthesis has afforded a number of NMOFs with various metal/ligand combinations, it has also led to amorphous gel-like materials for some combinations, presumably as a result of the rapid and irreversible metal-to-ligand bond formation. Lin et al. recently developed a surfactant-mediated hydrothermal method for the synthesis of NMOFs.[19] Elevated temperatures can alter the relative kinetics for nucleation and nanocrystal growth, favoring the formation of uniform nanomaterials under hydrothermal conditions.

NMOFs of the composition $Gd_2(bhc)(H_2O)_6$ were prepared by heating a mixture of hexa(methylammonium) benzenehexacarboxylate (bhc) and $GdCl_3$ in a microemulsion composed of CTAB, 1-hexanol, heptane, and water at 120 °C.[19] The resulting block-like particles with dimensions of approximately $25 \times 50 \times 100$ nm corresponded to a known crystalline lanthanum analog with the fluorite network topology (Figure 5).

Interestingly, nanorods of $[Gd_2(bhc)(H_2O)_8]\cdot 2H_2O$ were obtained by reacting $GdCl_3$ and mellitic acid (H_6bhc) in the same microemulsion system at 60 °C in a microwave reactor.[19] Electron micrographs showed that the nanorods were 100–300 nm in diameter and several microns in length (Figure 6a–b). X-ray structure studies revealed that each Gd center coordinates to two chelating carboxylates and one monodentate carboxylate from three different bhc ligands and four water molecules. The bhc ligand acts as a six-connected node whereas the Gd center acts as a three-connected node to form a 3D framework with the rutile network topology (Figure 6c–e).

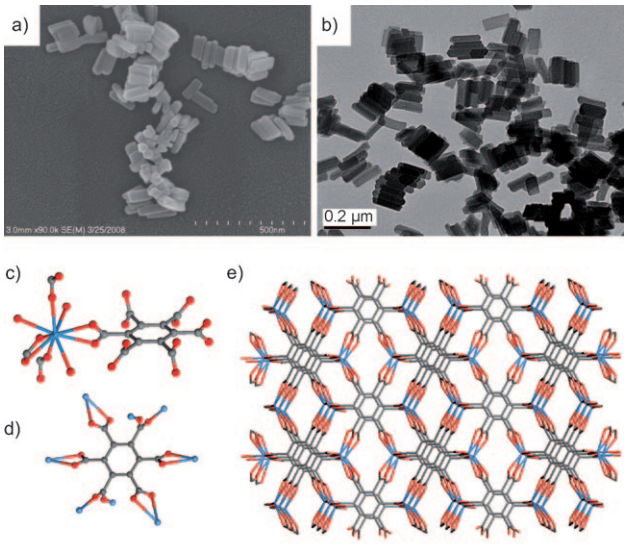

Figure 5. a) SEM and b) TEM micrographs of $Gd_2(bhc)(H_2O)_6$. c)–e) Crystal structures illustrating the Gd coordination environment, linking of bhc to eight different Gd centers, and packing in $Gd_2(bhc)(H_2O)_6$, respectively. Structures were drawn using the cif file for isostructural $La_2(bhc)(H_2O)_6$.[19]

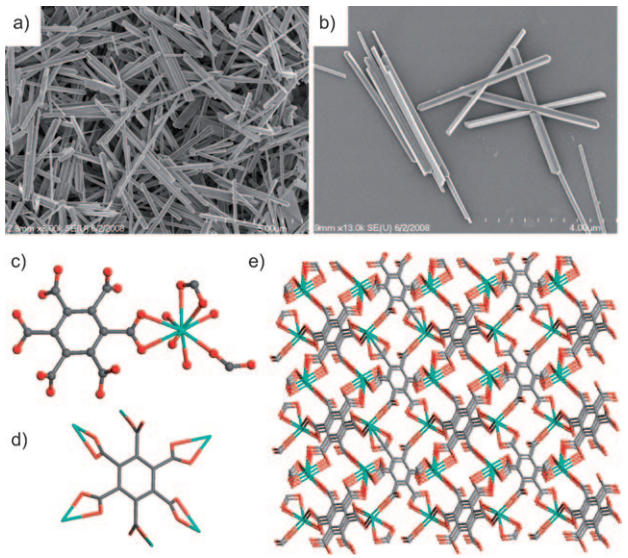

Figure 6. a) and b) SEM micrographs of $[Gd_2(bhc)(H_2O)_8]\cdot 2H_2O$. c)–e) Crystal structures illustrating the Gd coordination environment, linking of bhc to eight different Gd centers, and packing in $Gd_2(bhc)(H_2O)_8]\cdot 2H_2O$, respectively.[19]

The synthesis of two different NMOFs based on the Gd/bhc building blocks is a result of the different metal-ligand coordination modes. Coordination isomerism in this system is pH-dependent but not temperature-dependent. This work illustrates the ability to synthesize different NMOFs from the same metal/ligand combination by exploiting versatile metal-ligand coordination modes.

Jung and Oh recently reported a solvothermal method for NMOF synthesis and closely monitored the particle morphological transformation during the synthesis (Figure 7).[20] A

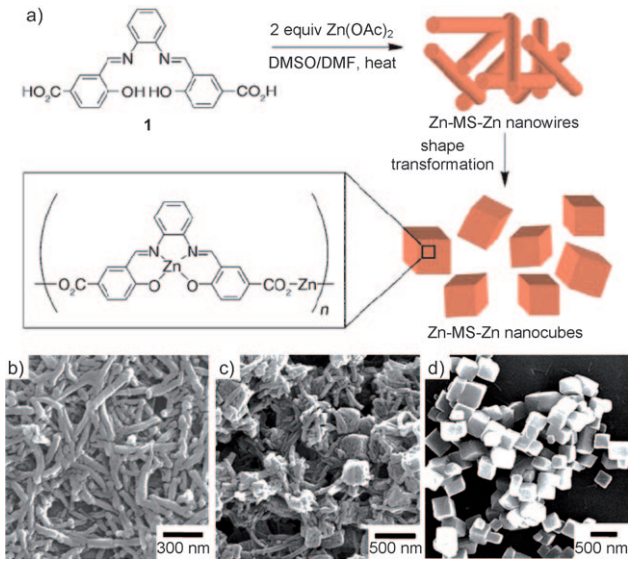

Figure 7. a) Scheme for the synthesis of Zn–MS–Zn nanowires and their subsequent transformation into nanocubes (MS=metalated salen). b)–d) SEM micrographs illustrating the transformation of nanowires into nanocubes during the synthesis.[20]

solution of *N*,*N*′-phenylenebis(salicylideneimine)dicarboxylic acid in DMSO was added to a DMF solution containing two equivalents of $Zn(OAc)_2$. One equivalent of the Zn ions coordinates to the salen pocket, while the other connects the resulting metalloligands. The resulting solution was heated at 120 °C for 60 min, over which time nanowires transformed into nanocubes by aggregation and intrastructural fusion. They also demonstrated that the sizes of the nanocubes could be tuned by varying the reaction conditions: smaller particles were obtained when the solubility of the nanowires was decreased by either lowering the temperature or using a poorer solvent mixture.

3. Applications of Nanoscale Coordination Polymers

As nanoscale coordination polymers can be built from a wide selection of metal ions and an infinite number of organic bridging ligands, they can be engineered with an unprecedented range of compositions and properties. This high degree of tailorability has led to the synthesis of a large number of NCP and NMOF materials. More importantly, they have been shown to exhibit interesting characteristics for a variety of applications, including catalysis, spin-crossover, templating, biological sensing and multimodal biomedical imaging, and drug-delivery.

3.1. Heterogeneous Catalysis

Heterogeneous catalysts often display size-dependent physical and chemical properties because the activity depends on surface area and substrate transport. The immobilization of organometallic complexes by their incorporation into self-supported networks, such as NCPs, is a particularly promising

strategy to formulate materials with a high density of catalytically active sites. Sweigart and Son's organometallic nanocatalyst (ON) based on the $[(\eta^4\text{-}1,4\text{-quinone})Rh(cod)]^-$ linker unit catalyzed the stereoselective polymerization of phenylacetylene.[10] The size-dependent catalytic properties of ONs are clearly summarized in Table 1. Smaller particles yielded longer poly(phenylacetylene) polymers owing to increased catalytic activity. Moreover, the ONs, of various particle sizes, were much more stereoselective than the molecular organorhodium catalyst.

Table 1: Polymerization of phenylacetylene catalyzed by ONs.[10]

Catalyst[a]	Solvent	M_n	M_w/M_n	Yield [%]	Selectivity [%][b]
1$^+$[a]	CH_2Cl_2	2900	1.8	90	59
ON1[c]	CH_2Cl_2	4100	4.3	82	86
ON2[d]	CH_2Cl_2	13200	3.4	84	94
ON3[e]	CH_2Cl_2	15600	3.5	86	96
1$^+$	THF	17800	2.4	98	59
ON1	THF	23600	1.8	88	95
ON2	THF	26800	2.2	98	95
ON3	THF	29200	2.2	98	96

[a] $[(\eta^6\text{-}1,4\text{-hydroquinone})Rh(cod)]^+$. [b] *cis*-poly(phenylacetylene) content. [c] 537 nm particles. [d] 402 nm particles. [e] 340 nm particles.

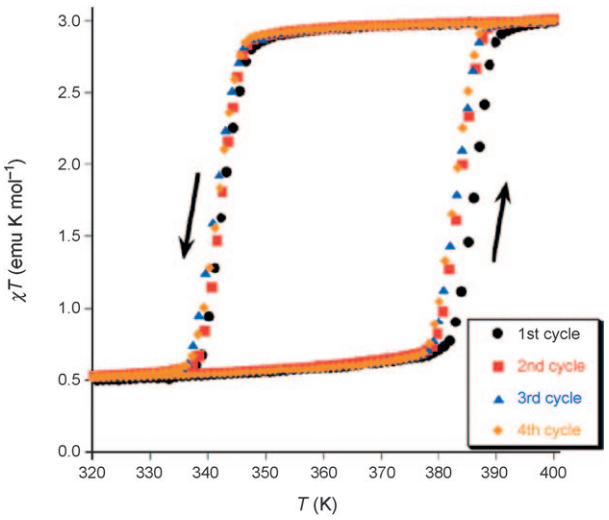

Figure 8. Magnetic thermal hysteresis for $[Fe(Htrz)_2(trz)](BF_4)$ nanoparticles.[18]

3.2. Spin-Crossover

Spin-crossover is a phenomenon whereby a material transitions from a low-spin configuration to a low-lying metastable high-spin configuration as a result of external stimuli, such as temperature or light-irradiation. Octahedral Fe^{II} compounds with the $3d^6$ electronic configuration are among the most extensively studied spin-crossover systems. The $[Fe(Htrz)_2(trz)](BF_4)$ nanoparticles prepared by Coronado et al. displayed a thermally-induced low to high spin transition almost identical to that reported for the bulk sample (Figure 8).[18] This transition is accompanied by a drastic color change from deep purple/red to light pink or white, which has previously been utilized in the development of write/read technologies. Similar spin-crossover behavior was seen in the NCPs prepared by Ruiz-Molina et al.[15] The nanoparticles with a low-spin $[Co^{III}(3,5\text{-dbsq})(3,5\text{-dbcat})]$ configuration could be thermally transformed to the high-spin $[Co^{II}(3,5\text{-dbsq})_2]$ material. More recently, Gaspar, Real, and co-workers described the synthesis of bimetallic NMOFs $[Fe(pz)Pt(CN)_4]\cdot x H_2O$ (pz = pyrazine, $x = 1$ or 2.5) that exhibit magnetic, optical, and structural bistability near room temperature.[21] The bistability of these spin-crossover nanoparticles makes them attractive candidates for active components in a variety of multifunctional materials, and particularly in memory devices.

3.3. Templating with NMOFs

Core-shell nanostructures can exhibit interesting properties that result from both the templating core and the coating layer. Lin et al. demonstrated the utility of NMOFs as a template for the synthesis of novel core-shell nanostructures.[22] NMOFs were first coated with polyvinylpyrollidone (PVP) to reduce particle aggregation in solution. The PVP-functionalized intermediates were then treated with tetraethylorthosilicate (TEOS) in an ammonia/ethanol mixture to give nanocomposites with a NMOF core and a silica shell. The silica shell thickness could be tuned by varying the reaction time or by adjusting the amount of TEOS added to the reaction mixture.

The NMOF core could be completely removed (by dissolution) at low pH to afford hollow silica shells with varied thickness and aspect ratios. Since the morphologies of NMOFs can be controlled by exploiting the energetics of different crystallographic faces, such a templating approach can be used to produce interesting nanoshells that are not accessible with presently available methods. For example, silica nanoshells with a very high aspect ratio of 40 were synthesized using $[Gd_2(bdc)_3(H_2O)_4]$ NMOF as the template (Figure 9).

The silica shell of such nanocomposites also significantly stabilized the NMOF core against dissolution. The dissolution curves for as-synthesized and silica-coated $Gd_2(bdc)_3(H_2O)_4$ NMOFs had a zeroth-order rate constant of 0.143 $\mu M\,h^{-1}$ and 0.084 $\mu M\,h^{-1}$ at pH 4, respectively. These results indicate that the rates of cargo release from such core-shell nanostructures can be readily controlled by taking advantage of slow diffusion of metal and organic constituents through the silica shell.

Silica as a surface coating offers several additional advantages, including enhanced water dispersibility, biocompatibility, and the ease of further functionalization with a variety of silyl-derived molecules. As shown below, the nanocomposites with NCP or NMOF cores and silica shells have been used for biosensing, multimodal imaging, and anticancer drug delivery.

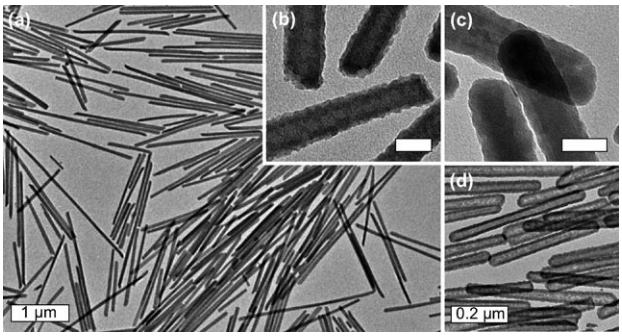

Figure 9. a) and b) TEM images of $Gd_2(bdc)_3(H_2O)_4$ NMOFs with a 2–3 nm silica shell; c) TEM image of $Gd_2(bdc)_3(H_2O)_4$ NMOFs with an 8–9 nm silica shell; d) TEM image of 8–9 nm hollow silica nanoshells generated from (c). Scale bars in (b) and (c) are 50 nm.[22]

3.4. Biosensing and Multimodal Imaging

Gd- and Mn-based NMOFs were shown to enhance image contrast in magnetic resonance imaging (MRI). MRI is a powerful non-invasive diagnostic technique that can differentiate normal tissue from diseased tissue based on variations of the water-proton NMR signals. These variations arise from differences in water density, tissue environment, and/or nuclear relaxation rates. Complexes of highly paramagnetic metal ions, such as Gd^{3+} and Mn^{2+}, are often administered to enhance image contrast by increasing the rate of water proton relaxation. By incorporating the metal ions or metal complexes into nanoparticles the rate of relaxation can be further increased owing to reduced rotational diffusion of the contrast agent. For example, $Gd_2(bdc)_3(H_2O)_4$ nanorods approximately 100 nm in length by 40 nm in diameter display a longitudinal relaxivity (r_1) value of 35.8 $mM^{-1}s^{-1}$, in an aqueous xanthan gum suspension (Table 2).[16] This value is almost an order of magnitude higher than that obtained with the commercially available T_1-weighted contrast agent Omniscan[16]. More importantly, the relaxivities on a per particle basis are extraordinarily high, owing to the presence of a very large number of Gd^{3+} centers in each particle, which would potentially allow them to be effective site-specific contrast agents when conjugated to the appropriate targeting moieties.

Table 2: MR relaxivities for Gd- and Mn-based NMOFs synthesized by our group.[a][16,17,19]

Compound	Ion r_1	Ion r_2
$Gd_2(bdc)_3(H_2O)_4$[b]	35.8	55.6
$Gd_2(bdc)_3(H_2O)_4$[c]	26.9	49.1
$Gd_2(bdc)_3(H_2O)_4$[d]	20.1	45.7
$[Gd(ibtc)(H_2O)_3]\cdot H_2O$	13.0	29.4
$Gd_2(bhc)(H_2O)_6$	1.5[e]	122.6[e]
$Mn(bdc)(H_2O)_2$	5.5	7.8
$Mn_3(btc)_2(H_2O)_6$	7.8	70.8

[a] Relaxivities were obtained at 3.0 Tesla and are given in $mM^{-1}s^{-1}$. [b] Nanoparticle size was approximately 100×40 nm. [c] Nanoparticle size was approximately 400×70 nm. [d] Nanoparticle size was approximately 1000×100 nm. [e] Values obtained at 9.4 Tesla.

NCPs and NMOFs can also be rendered luminescent by incorporating emissive metal ions or organic fluorophores (Figure 10). Gd NMOFs can be doped with the emissive lanthanide ions Eu^{3+} or Tb^{3+} to afford luminescent nanoparticles.[16] The organic linkers such as benzenedicarboxylic acid act as antenna to absorb light and transfer its excitation energy to the lanthanide ions. NCPs can be built from luminescent organic or organometallic linkers that have a high absorption coefficient and thus obviate the need for an antenna. The M–BMSB linker prepared by Mirkin gave an emission peak around 600 nm ($\lambda_{ex} = 420$ nm), and the M-BMSB-M′ particles were highly luminescent under ultraviolet irradiation.[12] The optical properties of these materials could also be fine-tuned by changing the ancillary ligands coordinating to the metal centers.

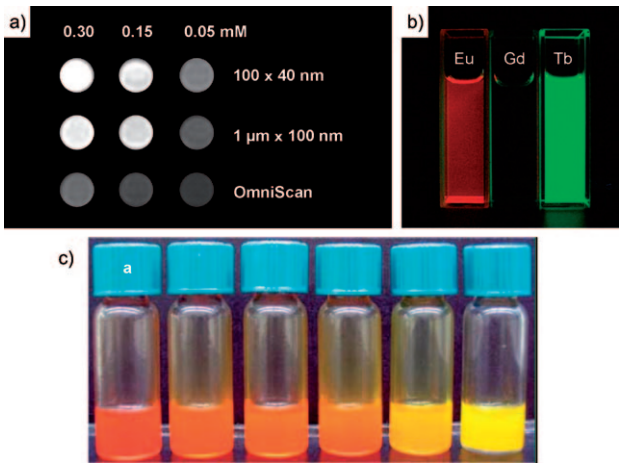

Figure 10. a) T_1-weighted MRI phantom images of suspensions of $Gd_2(bdc)_3(H_2O)_4$ NMOFs in water containing 0.1% xanthan gum as a dispersing agent. b) Luminescence of ethanolic dispersions of Eu- and Tb-doped $Gd_2(bdc)_3(H_2O)_4$ NMOFs when irradiated with UV light.[16] c) Luminescence of a series of Zn–BMSB–Zn particles in toluene with different ancillary ligands.[12]

NMOF-silica core-shell nanostructures were used for the ratiometric detection of the dipicolinic acid (DPA), a major constituent of spore-forming bacteria (such as anthrax), in solution (Figure 11). Eu-doped $Gd_2(bdc)_3(H_2O)_4$@SiO_2 core-shell nanoparticles were functionalized with a silylated Tb–edta moiety.[22] Whereas the Eu-doped NMOFs were inherently luminescent, the sensitized emission from Tb was dependent upon the complexation of DPA. The Tb luminescence signal thus provided a sensitive probe for DPA detection, whereas the Eu emission from the NMOF core acted as a non-interfering internal calibration.

NMOF-silica nanostructures were recently functionalized with rhodamine B and a targeting peptide for cancer imaging. Confocal fluorescence microscopy and MRI studies indicated that the cyclic-(RGDfK)-targeted particles with the $Mn_3(btc)_2(H_2O)_6$ NMOF core and silica shell exhibited enhanced uptake by angiogenic human colon carcinoma (HT–29) cells, as compared to non-targeted particles (Figure 12).[17] NCPs and NMOFs thus provide an interesting platform for design-

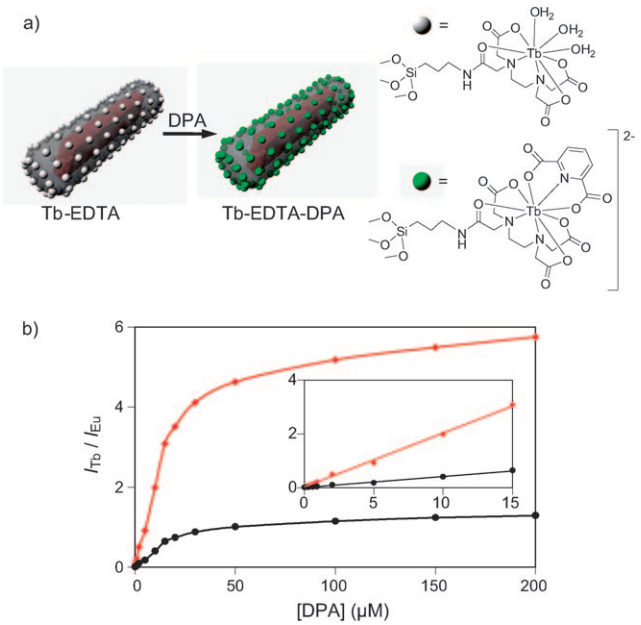

Figure 11. a) Schematic showing luminescence sensing of dipicolinic acid using core-shell nanostructures. b) Ratiometric curves obtained by plotting the Tb/Eu luminescence signal intensities exhibited by Tb–edta-functionalized $Gd_{1.96}Eu_{0.04}(bdc)_3(H_2O)_4$ against DPA concentration (red = 544 nm/592 nm, black = 544 nm/615 nm). The inset shows the linear relationship at low DPA concentrations.[22]

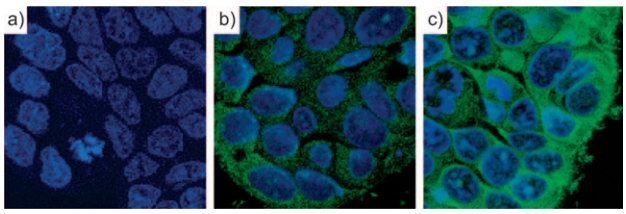

Figure 12. Merged confocal images of HT–29 cells that were incubated with a) no $Mn_3(btc)_2(H_2O)_6$/silica core-shell nanostructures, b) non-targeted $Mn_3(btc)_2(H_2O)_6$/silica core-shell nanostructures, c) cyclic-(RGDfK)-targeted $Mn_3(btc)_2(H_2O)_6$/silica core-shell nanostructures. The blue color was from DRAQ5 used to stain the cell nuclei, whereas the green color was from rhodamine B.

ing multifunctional nanomaterials for biosensing and biomedical imaging.

3.5. Drug Delivery

As described in Section 3.3, the silica shell in the NMOF–silica nanocomposite stabilized the NMOF core and allowed for control of the cargo release rate by varying the silica shell thickness. Lin et al. used this strategy to effectively deliver anticancer drugs.[13] The NCPs based on the DSCP and Tb^{III} building blocks were first coated with a silica shell. The half-life ($t_{1/2}$) for the release of DSCP, an analog of the anticancer drug cisplatin, from NCPs of the composition $Tb_2(DSCP)_3(H_2O)_{12}$ could be tuned from approximately 5.5 h to 9 h by increasing the shell thickness from approximately 2 nm to 7 nm. In comparison, the as-synthesized NCPs had a $t_{1/2}$ for dissolution of only 1 h. In vitro cytotoxicity assays showed that the Pt-based NCP particles displayed anticancer efficacies superior to the cisplatin standards (Figure 13). These

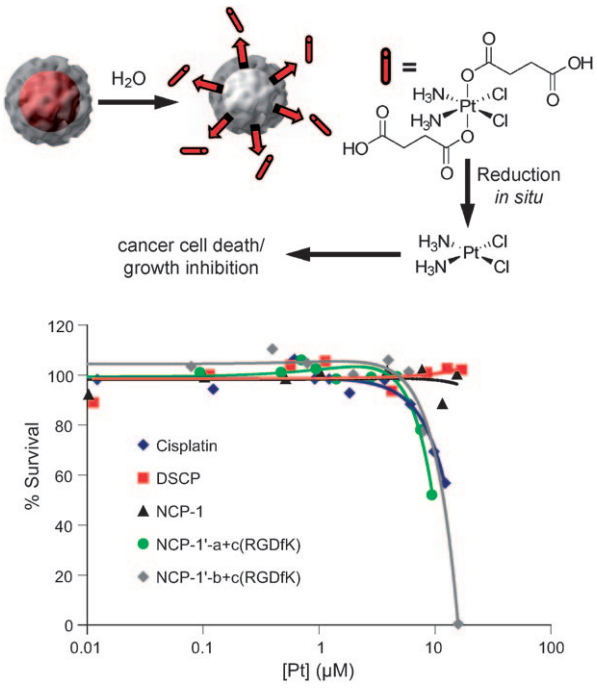

Figure 13. a) Schematic showing controlled release of DSCP from the core-shell nanostructure. b) In vitro cytotoxicity assay curves for HT–29 cells incubated with various Pt-based NCPs.[13]

results were significant because they clearly demonstrated the feasibility of using NCPs as delivery vehicles for clinically relevant cargos.

4. Summary and Outlook

The past few years have witnessed the synthesis of nanoscale coordination polymers of both amorphous (NCP) and crystalline (NMOF) nature. They have been synthesized by a variety of techniques, including precipitation by combining metal and organic components, precipitation by antisolvent addition, microemulsion synthesis, surfactant-mediated synthesis, and hydrothermal synthesis. New synthetic strategies are still needed in order to take full advantage of the limitless number of possible formulations of NCPs and NMOFs.

The utility of many of the NCPs and NMOFs has been demonstrated in a number of interesting applications, such as catalysis, spin-crossover, templating, biosensing, biomedical imaging, and anticancer drug delivery. This class of nanomaterials allows for the exploration of many other applications by taking advantage of the ability to systematically tune the compositions using judicious choice of building blocks. A specific area that has received little attention, but could provide great advantages, is the scaling down of catalytically

active MOFs to the nano-regime, greatly altering the diffusion kinetics, and resulting in much more efficient heterogeneous catalysts. We believe that modular synthesis of nanoscale coordination polymers can lead to a new generation of functional nanomaterials based on molecular components.

We thank NSF and NIH for supporting our research.

Received: July 12, 2008
Published online: December 9, 2008

[1] M. Haruta, *Chem. Rev.* **2003**, *103*, 75 – 87.
[2] V. I. Klimov, S. A. Ivanov, J. Nanda, M. Achermann, I. Bezel, J. A. McGuire, A. Piryatinski, *Nature* **2007**, *447*, 441 – 446.
[3] a) I. Gur, N. A. Fromer, M. L. Geier, A. P. Alivisatos, *Science* **2005**, *310*, 462 – 465; b) M. Grätzel, *Inorg. Chem.* **2005**, *44*, 6841 – 6851.
[4] a) X. Gao, Y. Cui, R. M. Levenson, L. W. Chung, S. Nie, *Nat. Biotechnol.* **2004**, *22*, 969 – 976; b) C. Sönnichsen, B. M. Reinhard, J. Liphardt, A. P. Alivisatos, *Nat. Biotechnol.* **2005**, *23*, 741 – 745; c) S. E. Skrabalak, J. Chen, Y. Sun, X. Lu, L. Au, C. M. Cobley, Y. Xia, *Acc. Chem. Res.* **2008**, DOI: 10.1021/ar800018v.
[5] a) M. Vallet-Regí, F. Balas, D. Arcos, *Angew. Chem.* **2007**, *119*, 7692 – 7703; *Angew. Chem. Int. Ed.* **2007**, *46*, 7548 – 7558; b) L. Zhang, F. X. Gu, J. M. Chan, A. Z. Wang, R. S. Langer, O. C. Farokhzad, *Clin. Pharmacol. Ther.* **2008**, *83*, 761 – 769.
[6] W. R. Entley, G. S. Girolami, *Science* **1995**, *268*, 397 – 400.
[7] a) S. Vaucher, M. Li, S. Mann, *Angew. Chem.* **2000**, *112*, 1863; *Angew. Chem. Int. Ed.* **2000**, *39*, 1793; b) S. Vaucher, J. Fielden, M. Li, E. Dujardin, S. Mann, *Nano Lett.* **2002**, *2*, 225 – 229; c) L. Catala, T. Gacoin, J. P. Boilot, E. Riviere, C. Paulsen, E. Lhotel, T. Mallah, *Adv. Mater.* **2003**, *15*, 826; d) T. Uemura, S. Kitagawa, *J. Am. Chem. Soc.* **2003**, *125*, 7814 – 7815; e) P. A. Fiorito, V. R. Goncales, E. A. Ponzio, S. I. C. de Torresi, *Chem. Commun.* **2005**, 366 – 368; f) M. Taguchi, K. Yamada, K. Suzuki, O. Sato, Y. Einaga, *Chem. Mater.* **2005**, *17*, 4554 – 4559; g) T. Uemura, S. Kitagawa, *Chem. Lett.* **2005**, *34*, 132 – 137.
[8] a) S. Kitagawa, R. Kitaura, S. Noro, *Angew. Chem.* **2004**, *116*, 2388 – 2430; *Angew. Chem. Int. Ed.* **2004**, *43*, 2334 – 2375; b) C. Wu, W. Lin, *Angew. Chem.* **2007**, *119*, 1093; *Angew. Chem. Int. Ed.* **2007**, *46*, 1075; c) O. R. Evans, W. Lin, *Acc. Chem. Res.* **2002**, *35*, 511.
[9] X. P. Sun, S. J. Dong, E. K. Wang, *J. Am. Chem. Soc.* **2005**, *127*, 13102 – 13103.
[10] K. H. Park, K. Jang, S. U. Son, D. A. Sweigart, *J. Am. Chem. Soc.* **2006**, *128*, 8740 – 8741.
[11] a) A. Hu, H. L. Ngo, W. Lin, *Angew. Chem.* **2003**, *115*, 6182 – 6185; *Angew. Chem. Int. Ed.* **2003**, *42*, 6000 – 6003; b) A. Hu, H. L. Ngo, W. Lin, *J. Am. Chem. Soc.* **2003**, *125*, 11490 – 11491.
[12] a) M. Oh, C. A. Mirkin, *Nature* **2005**, *438*, 651 – 654; b) M. Oh, C. A. Mirkin, *Angew. Chem.* **2006**, *118*, 5618 – 5620; *Angew. Chem. Int. Ed.* **2006**, *45*, 5492 – 5494.
[13] W. J. Rieter, K. M. Pott, K. M. L. Taylor, W. Lin, *J. Am. Chem. Soc.* **2008**, *130*, 11584 – 11585.
[14] H. Maeda, M. Hasegawa, T. Hashimoto, T. Kakimoto, S. Nishio, T. Nakanishi, *J. Am. Chem. Soc.* **2006**, *128*, 10024 – 10025.
[15] I. Imaz, D. Maspoch, C. Rodriguez-Blanco, J. M. Perez-Falcon, J. Campo, D. Ruiz-Molina, *Angew. Chem.* **2008**, *120*, 1883 – 1886; *Angew. Chem. Int. Ed.* **2008**, *47*, 1857 – 1860.
[16] W. J. Rieter, K. M. L. Taylor, H. An, W. Lin, W. Lin, *J. Am. Chem. Soc.* **2006**, *128*, 9024 – 9025.
[17] K. M. L. Taylor, W. J. Rieter, W. Lin, *J. Am. Chem. Soc.* **2008**, *130*, 14358 – 14358.
[18] E. Coronado, J. R. Galan-Mascaros, M. Monrabal-Capilla, J. Garcia-Martinez, P. Pardo-Ibanez, *Adv. Mater.* **2007**, *19*, 1359.
[19] K. M. L. Taylor, A. Jin, W. Lin, *Angew. Chem.* **2008**, *120*, 7836 – 7839; *Angew. Chem. Int. Ed.* **2008**, *47*, 7722 – 7725.
[20] S. Jung, M. Oh, *Angew. Chem.* **2008**, *120*, 2079 – 2081; *Angew. Chem. Int. Ed.* **2008**, *47*, 2049 – 2051.
[21] I. Boldog, A. B. Gaspar, V. Martínez, P. Pardo-Ibanez, V. Ksenofontov, A. Bhattacharjee, P. Gutlich, J. A. Real, *Angew. Chem.* **2008**, *120*, 6533 – 6537; *Angew. Chem. Int. Ed.* **2008**, *47*, 6433 – 6437.
[22] W. J. Rieter, K. M. L. Taylor, W. Lin, *J. Am. Chem. Soc.* **2007**, *129*, 9852 – 9853.

